

UC Berkeley

UC Berkeley Previously Published Works

Title

Positive spin Hall magnetoresistance in single-crystalline Pt/CoO(001) bilayers

Permalink

<https://escholarship.org/uc/item/7z08n2d3>

Journal

Physical Review B, 106(13)

ISSN

2469-9950

Authors

Xu, Jia

Jia, Mengwen

Zhou, Chao

et al.

Publication Date

2022-10-01

DOI

10.1103/physrevb.106.134425

Peer reviewed

---

# Positive spin Hall magnetoresistance in single crystalline Pt/CoO(001) bilayers

Jia Xu<sup>1,2,#</sup>, Mengwen Jia<sup>2,#</sup>, Chao Zhou<sup>1,2</sup>, Qian Li<sup>3</sup>, Padraic Shafer<sup>4</sup>,  
Gong Chen<sup>5</sup>, Mengmeng Yang<sup>6</sup>, Alpha T. N' Diaye<sup>4</sup>, Elke Arenholz<sup>4</sup>,  
Ziqiang Qiu<sup>7</sup> and Yizheng Wu<sup>2,8,\*</sup>

<sup>1</sup>*Department of Physics, School of Physics and Telecommunication Engineering, Shaanxi University of Technology, Hanzhong 723001, China*

<sup>2</sup>*Department of Physics and State Key Laboratory of Surface Physics, Fudan University, Shanghai 200433, China*

<sup>3</sup>*National Synchrotron Radiation Laboratory, University of Science and Technology of China, Hefei, Anhui 230029, China*

<sup>4</sup>*Advanced Light Source, Lawrence Berkeley National Laboratory, Berkeley, California 94720, USA*

<sup>5</sup>*Department of Physics, Georgetown University, Washington, DC 20057, USA*

<sup>6</sup>*Institute of Physical Science and Information Technology, Anhui University, Hefei, Anhui 230601, China*

<sup>7</sup>*Department of Physics, University of California at Berkeley, Berkeley, CA 94720, USA*

<sup>8</sup>*Shanghai Research Center for Quantum Sciences, Shanghai 201315, China*

## Abstract

The spin Hall magnetoresistance (SMR) effect in single crystalline Pt/CoO(001) bilayers has been systematically investigated. X-ray magnetic linear dichroism measurements prove that CoO antiferromagnetic (AFM) spins can be switched into the direction orthogonal to the applied field. We find the SMR signal is comprised of two components related to either the switching of CoO AFM Néel order or the applied strong field effect. Both SMR components show a “positive” angular dependence with  $R_{\parallel} > R_{\perp}$ , while  $R_{\parallel}$  ( $R_{\perp}$ ) being defined as the resistance with the applied in-plane field parallel (perpendicular) to the current. The observed positive SMR is mainly attributed to the uncompensated spins at the Pt/CoO interface, instead of the CoO AFM spins. Our study may attract great interest to understand the complicated SMR effect in AFM spintronics materials.

---

## I. Introduction

The discovery of spin Hall magnetoresistance (SMR) in Pt/Y<sub>3</sub>Fe<sub>5</sub>O<sub>12</sub> (YIG) [1,2] has attracted great interest in the last decade, since SMR provides a powerful tool to electrically monitor the magnetization direction in a magnetic insulator/heavy metal (HM) heterostructure. SMR has been widely investigated in magnetic systems of HM/ferromagnetic insulator (FMI) [1-6] or HM/ferromagnetic metal (FMM) [7-9], and was utilized to probe surface magnetization [10] and to resolve exotic magnetic phases such as spin canting [11] and helical magnetic order [12]. Recent studies in HM/antiferromagnetic insulator (AFMI) systems also demonstrated that SMR is sensitive to the antiferromagnetic (AFM) Néel order orientation [13-15], and can be applied to identify the current-induced switching of AFM Néel order [16-19].

SMR arises from the combined action of the spin Hall effect (SHE) [20,21] and the inverse spin Hall effect (ISHE). Therefore, it contains rich physical processes inside [1,2]. For the charge current  $J$  flowing in the HM layer, SHE can convert it into spin current, which can be further absorbed or reflected by the adjacent magnetic layer. The reflection of spin current depends on the relative angle between its polarization and the spin orientation in the magnetic layer. The reflected spin current produces an additional charge current by ISHE, thus the electrical resistance changes with the field orientation. Therefore, the electrical resistance depends on the relative angle between the applied current and the magnetization direction of the FM layer. In HM/FMI or HM/FMM bilayers, the magnetic spins should be aligned with the external field, thus SMR has the angular dependence of  $R_{\parallel} > R_{\perp}$  in most FM systems with  $R_{\parallel} (R_{\perp})$  defined as the longitudinal resistance with the applied in-plane field  $H$  parallel (perpendicular) to the current  $J$  [1-9].

However, in HM/ AFMI systems without the net magnetic moment, the AFM Néel order is usually believed to be aligned perpendicular to  $H$ , thus a negative SMR with  $R_{\parallel} < R_{\perp}$  is expected [15]. Such negative SMR was indeed observed in many HM/AFMI systems, such as Pt/NiO [14-17,22-25] and Pt/Fe<sub>2</sub>O<sub>3</sub> [18,26]. On the other hand, a positive SMR with  $R_{\parallel} > R_{\perp}$  has also been observed in many systems, such as

---

HM/Cr<sub>2</sub>O<sub>3</sub> [27-31] and Pt/CoO/Pt [32]. So, it still requires further investigations to unveil the mechanism of SMR in HM/AFMI systems, which should be of great importance to understand spin-dependent transport properties in AFM spintronics systems. Note that most SMR measurements in HM/AFMI systems were performed under strong magnetic field with the field strength up to several Tesla [14,32], and such strong fields could induce certain net magnetic spins, which further induce the SMR signal [33]. Thus, in order to better understand the mechanism of SMR in HM/AFMI systems, it is required to separate the contribution from the AFM Néel order and the field-induced net spins in the AFM layer.

CoO(001) film has been considered as a model system to investigate the properties of AFM domains [34-36] and the magnetic interaction in FM/AFM systems [37-39]. Although transverse resistance has been applied to investigate current-induced AFM domain switching [19,40], investigation on the SMR effect in HM/CoO(001) systems is still lacking. In this paper, we report our systematic studies on SMR in single crystalline Pt/CoO(001) bilayers. We first demonstrate that the CoO AFM Néel order can be driven perpendicular to the strong magnetic field at certain temperatures by utilizing X-ray magnetic linear dichroism (XMLD) measurement. A positive SMR signal was found in Pt/CoO(001) bilayers over a wide temperature range from 10 K to 300 K. The measured SMR signal is comprised of two components, related to the field-induced spins and the switching of CoO AFM Néel order, and both contributions show a positive SMR, which can be interpreted by uncompensated spins at the Pt/CoO interface. Our studies reveal the complicated effect of AFM spins on SMR, which could be helpful for understanding spin-dependent transport properties in AFM spintronics devices.

## II. Experiments

Single crystalline Pt/CoO(001) bilayers were prepared by molecular beam epitaxy in an ultrahigh vacuum (UHV) system Error: Reference source not found. MgO(001) single-crystal substrates were prepared by annealing at 600 °C for 30

---

minutes in the UHV system. Then, a 10 nm MgO seed layer was grown at 500 °C to improve the surface quality. The CoO layer was epitaxied by evaporating Co under an oxygen pressure of  $2 \times 10^{-7}$  Torr at room temperature (RT). All the samples were capped with a thin Pt layer as a conducting layer by pulse laser deposition at RT. Film thickness was determined by the deposition rate, which was monitored with a calibrated quartz thickness monitor. Sharp reflection high energy electron diffraction patterns reveal excellent epitaxy growth of CoO film with a lattice relation of CoO[100](001)//MgO[100](001) [38,41].

XMLD measurements were taken at the superconducting magnet endstation of beamline 4.0.2 of advanced light source. The field in this endstation can be applied along arbitrary directions with a maximum value of 4 T, and the sample temperature can be varied in the range of 78-330 K. As shown in Fig. 1(a), the XMLD effect was determined with the normally incident X-ray by changing the angle  $\varphi$ , which is defined as the angle between the X-ray polarization  $\hat{E}$  and the CoO [110] direction. The X-ray absorption spectrum (XAS) of the Co<sup>2+</sup>  $L_3$  edge was measured in the total electron yield mode by measuring the sample current.

The magnetoresistance (MR) was determined by the magneto-transport measurements using a physical properties measurement system (PPMS) from the Quantum Design company, which is equipped with a rotatable sample stage and a vertical magnetic field  $H$  with maximum value of 9 T. The Pt/CoO(001) films were patterned into the Hall bars with 20  $\mu\text{m}$  in width and 100  $\mu\text{m}$  in length with the current  $J$  flowing along the CoO [110] axis, as shown in Fig. 2(a), to perform standard four-probe measurements. The sample can be rotated during the measurement, so that the applied field  $H$  can be aligned along different directions with respect to the current flow. The resistance was measured using Delta mode with a Keithley 6221 current source and a Keithley 2182A nanovoltmeter, and the applied current was 1 mA.

### III. Results and discussion

#### A. The switching of CoO AFM Néel order measured by XMLD

---

It is well known that CoO has the G-type AFM spin structure, and the CoO(001) surface is spin compensated. The AFM CoO spins lie in the film plane for CoO films grown on MgO(001) surfaces with easy axis along  $\langle 110 \rangle$  directions [36,38]. Thus, if a strong magnetic field is applied along  $\langle 110 \rangle$  directions, it is expected that the AFM spins can be aligned perpendicular to the field due to spin-flop coupling between applied fields and AFM ordered spins.

We performed the XMLD measurements at the Co  $L_3$  edge to directly determine whether a strong field can switch the AFM spin direction in a CoO (001) film with 4 nm thickness. In order to avoid the charging effect during the XMLD measurements, the sample was capped by a 1.2-nm-thick Pt layer. First, we studied the AFM CoO spins aligned by the field cooling process. The sample was cooled from 330 K down to 100 K with cooling field  $H_{FC} = 4$  T along CoO[110]. Then, the typical XAS of the Co<sup>2+</sup>  $L_3$  edge at normal incidence was measured at zero field with the X-ray polarization  $\hat{E}$  parallel to CoO  $[1\bar{1}0]$  ( $\varphi = 0^\circ$ ) and CoO  $[110]$  ( $\varphi = 90^\circ$ ) at 100 K shown as Fig. 1(b). It clearly shows the existence of the XMLD effect at low temperature, while the intensity of the second peak located at  $h\nu \sim 777.4$  eV is higher for  $\varphi = 0^\circ$  than for  $\varphi = 90^\circ$ . Fig. 1(c) shows the absence of the XMLD effect at  $T = 320$  K above the Néel temperature of CoO film, which confirm the magnetic origin of the observed XMLD effect. We further repeated the same measurement with  $H_{FC}$  along the  $[1\bar{1}0]$  direction, which is another easy axis of CoO(001) film. The obtained XAS shows the XMLD effect opposite to that in Fig. 1(b), which clearly indicates that field cooling can align the AFM CoO spins.

After field cooling, we systematically studied the XAS as a function of  $\varphi$  by rotating the X-ray polarization  $\hat{E}$ , and quantified the XMLD effect with the  $L_3$  ratio ( $R_{L_3}$ ), which is defined as the ratio of the XAS intensities at 777.4 and 777.9 eV [marked as  $I_1$  and  $I_2$  in Fig. 1(b), respectively]. Fig. 1(d) shows the  $\varphi$ -dependent  $R_{L_3}$  values for two orthogonal cooling fields, which shows the opposite behavior and can be well fitted by the  $\cos(\varphi)$  function. According to results in the literature [38,42], the

$R_{L_3}$  value for  $\dot{E} \perp \dot{S}_{CoO}$  should be smaller than that for  $\dot{E} \parallel \dot{S}_{CoO}$ , so the AFM CoO spin  $\dot{S}_{CoO}$  can be determined as  $\dot{S}_{CoO} \parallel [110]$  for  $H_{FC} \parallel [1\bar{1}0]$ , and  $\dot{S}_{CoO}$  along  $[1\bar{1}0]$  for  $H_{FC} \parallel [110]$ . Thus, our results conclude that CoO AFM spins can be aligned to a single domain state with the AFM spin  $\dot{S}_{CoO}$  perpendicular to  $H_{FC}$ , due to the perpendicular coupling between the CoO AFM spins and the external fields.

In order to further study the field driven AFM CoO spin switching process, after the CoO is initialized into the state with  $\dot{S}_{CoO} \perp H_{FC}$  by field cooling, we performed the XMLD measurements under a strong field  $H$  perpendicular to  $H_{FC}$ . Figure 1(e) shows the temperature dependence of the  $L_3$  ratio difference  $\Delta R_{L_3}$  ( $\Delta R_{L_3}^{\phi=0^\circ} - \Delta R_{L_3}^{\phi=90^\circ}$ ) under a field of 4 T. For the initial AFM spin states with  $H_{FC} \parallel [110]$ ,  $\Delta R_{L_3}$  decreases with the temperature, and changes sign across zero at  $\sim 240$  K, indicating a spin-flop transition of CoO AFM spins. Due to the magnetic interaction between the  $Co^{2+}$  spins and the external field, the  $Co^{2+}$  AFM spins perpendicular to  $H$  will have lower energy, thus the applied strong field could induce AFM spin switching assisted by thermal activation at certain temperatures. For the initial AFM spins states with  $H_{FC} \parallel [1\bar{1}0]$ , the temperature-dependent  $\Delta R_{L_3}$  shows a similar trend despite the opposite sign. We also found that the XMLD signal gradually vanishes at  $\sim 310$  K, which further confirms the magnetic origin of the observed XMLD effect [38,42].

Fig. 1(e) demonstrates that the CoO AFM spins can be switched by a 4 T field at  $\sim 240$  K, and it can be switched by a lower field at higher temperature. Fig. 1(f) shows the field-dependent  $\Delta R_{L_3}$  with  $H \perp H_{FC}$  after the CoO film is initialized into a single domain state at 260 K by  $H_{FC}$ . The XMLD signal reverses the sign at  $H \sim 3.5$  T, indicating the  $90^\circ$  switching of CoO AFM spins induced by the spin-flop coupling. The change of the XMLD signal in Fig. 1(f) is gradual with the applied field, thus it is expected that a combined process of domain nucleation and domain wall propagation

---

occurs during the switching of CoO AFM spins [39,43].

### B. Angular dependent magnetoresistance in Pt/CoO bilayers

The switching of CoO Néel order may provide a good route to identify the relationship between SMR and the AFM spin states in Pt/CoO bilayers. The angular dependent magnetoresistance (ADMR) within a rotating field has proved an effective method to study the SMR effect [2]. The films of Pt(3 nm)/CoO(4 nm)/MgO(001) were patterned into the standard Hall bar by photolithography. While the current  $J$  is flowing along the CoO  $[1\bar{1}0]$  axis, as shown in Fig. 2(a)-(b), the longitudinal resistance  $R_{xx}$  is measured in a standard four-probe configuration. The ADMR measurements are performed by rotating the field  $H$  with the angle  $\alpha_{xy}$  in the  $xy$ -plane and with the angle  $\beta_{xz}$  in the  $xz$ -plane, respectively.

Figs. 2(c-e) show the typical ADMR curves under a rotating field of 9 T at 300 K, 100 K and 10 K, respectively. For the field rotating in the  $xy$ -plane,  $R_{xx}$  changes with the  $\cos^2(\alpha)$  function, and the amplitude increases with decreasing temperature. However, for the field rotating in the  $xz$ -plane,  $R_{xx}$  shows very slight change at  $T > 100$  K, so the ADMR shows a clear relation of  $R_{\parallel} \approx R_p > R_{\perp}$ , with  $R_p$  defined as the resistance with  $H$  normal to the film surface, and such angular dependence is similar to the positive SMR in the Pt/YIG system [1-4]. For  $T < 100$  K, the ratios of ADMR for the field rotating in both  $xz$ - and  $xy$ -planes increase with decreasing temperature, with the relationship of  $R_{\parallel} > R_p > R_{\perp}$ . As shown in Fig. 2(f), the ADMR in Pt/CoO bilayers increase nonlinearly with the applied field, and the ADMR ratio  $R/R_{\parallel} (= (R_{\parallel} - R_{\perp})/R_{\parallel})$  can reach  $5 \times 10^{-4}$  at 9 T if measured at 100 K.

The  $\alpha_{xy}$ -dependence of ADMR in the Pt/CoO bilayer reveals the characteristic signature of “positive” SMR similar to that in Pt/YIG bilayers [1-4], opposite to the SMR in Pt/NiO [14-17,25] and  $\alpha$ -Fe<sub>2</sub>O<sub>3</sub>/Pt systems [18,26]. Moreover, in most HM/AFMI systems, the measured SMR is usually less than  $4 \times 10^{-4}$  [14,25,31]. In the Pt/CoO/Pt trilayer system, Oda et al. also reported the positive SMR effect with a small ratio of  $8 \times 10^{-5}$  with a field up to 25 T [32]. However, the SMR ratio in the Pt/CoO(001) bilayer is much larger, which can reach up to  $1.3 \times 10^{-3}$  in Fig. 2.



---

### C. SMR related to the switching of AFM Néel order

Fig. 2 shows that the measured SMR signal increases with the field, and it is hard to distinguish between the SMR contribution from the applied field and that from the switching of CoO AFM spins. The XMLD measurements in Fig. 1 already demonstrate that the CoO AFM spins can be switched by the field at certain temperatures, which can be applied to identify the effect of AFM spin switching on SMR. Fig. 3(a) shows the ADMR measurement at 200 K from a Pt/CoO(4 nm) sample with the field rotated clockwise and counterclockwise in the xy-plane. The measured ADMR curves deviate from the *sine* function with a clear hysteresis for the field around the  $\langle 100 \rangle$  axis. Such SMR hysteresis clearly demonstrates the switching of the CoO AFM spins under the strong field. For the CoO grown on MgO(001), the CoO AFM spins have been determined along the CoO $\langle 110 \rangle$  directions [36,43], thus the  $\langle 100 \rangle$  axis is the hard axis of AFM spins. In order to overcome the crystalline energy barrier around the hard axis, the AFM spin switching should happen for the field rotating over the hard axis, forming the hysteresis loop.

The switching of the CoO AFM spins can be further electrically detected by the SMR effect through the field sweeping. As indicated by the XMLD measurements in Fig. 1, if the sample is cooled down with the field along x-axis parallel to the  $[1\bar{1}0]$  direction, the CoO AFM spins can be aligned along the y-axis (CoO  $[110]$ ) due to the spin-flop coupling. After removing the field, the AFM spins still align along the y-axis, as indicated by the state in Fig. 3(b). Then, as we gradually increase the field  $H_y$  along the y-axis, a rapid decrease of  $R_{xx}$  can be observed at  $H \sim 7.5$  T, indicating that the AFM spins switch to the x-axis (the state  $\uparrow$ ). When the field is decreased back to zero, the AFM spins still remain along the x-axis (the state  $\uparrow$ ). However, while increasing the field along the x-axis, one jump of  $R_{xx}$  can be observed at  $H \sim 8.2$  T due to the AFM spin switching to the state  $\downarrow$ . The resistance gradually changes back to the state  $\downarrow$  while decreasing the  $H_x$  field back to zero. The higher switching field while applying  $H_x$  may be attributed to the enhanced pinning effect after the first AFM domain switching

process while applying  $H_y$  [39]. Note that field-dependent ordinary magnetoresistance (OMR) also occurs in nonmagnetic metal Pt. However, the amplitude of OMR in our measurements has an upper limit of  $2 \times 10^{-4}$  at 9 T, as can be estimated by the resistance difference between state and subtracted by the difference between state and . The OMR is much smaller than the observed ADMR in Fig. 2 at low temperatures, so it will not affect the analysis in the previous section. So, Fig. 3(b) shows that  $R_{xx}$  at zero field with  $\dot{S}_{CoO} \parallel J$  is smaller than that with  $\dot{S}_{CoO} \perp J$ , corresponding to the relation of  $R_{\parallel} > R_{\perp}$  if considering the  $90^\circ$  coupling between the AFM spin and the magnetic field [2]. This positive SMR signal purely originates from AFM spin switching in the Pt/CoO system.

Fig. 3(b) also demonstrates that the strong magnetic field along the different directions can generate additional MR signal. In order to better identify the SMR signal due to the AFM spin switching, we subtract the MR signals between  $R_{H_y}^{0 \rightarrow 9T}$  and  $R_{H_y}^{9 \rightarrow 0T}$ , which represent the resistances for the field  $H_y$  increasing from 0 T to 9 T and decreasing from 9 T to 0 T, respectively. The obtained  $\Delta R_{H_y}(H) = R_{H_y}^{0 \rightarrow 9T}(H) - R_{H_y}^{9 \rightarrow 0T}(H)$  measured at 200 K in Fig. 3(c) show a clear decrease at  $H \sim 7.5$  T with a small field-dependent background. Similar MR measurements with field sweeping were also performed at different temperatures. There is a clear field-induced change of MR at temperatures between 180 K and 220 K, and the switching field  $H_s$  decreases with increasing temperature. Since  $H_s$  in the 4 nm CoO film is close to 9 T at 180 K, no AFM switching is expected below 180 K. The XMLD measurements in Fig. 1 demonstrate the switching of AFM CoO spins induced by the field below 4 T at  $\sim 240$  K. We plot the switching field  $H_s$  determined by both XMLD and SMR measurements on 4 nm CoO samples in Fig. 3(d).  $H_s$  decreases with the temperature, which can be extrapolated to zero at  $\sim 300$  K.

However, the SMR measurement at 260 K in Fig. 3(c) doesn't show any switching signal, since the field induced switching of CoO AFM spins should happen according to the XMLD measurement in Fig. 1, thus our results indicate that the observed SMR signal at zero field may not fully originate from the CoO AFM spins.

The AFM order after switching can be demonstrated to be very robust. At 200 K, we applied the field along the x-direction up to 9 T to switch the CoO AFM spins into the y-axis, and then decreased it to zero. Then the long-time resistance measurement in Fig. 4(a) demonstrates the stability of the AFM order after switching. We also did similar measurements with  $H$  along the y-direction, and the measured signal  $R_{0T}^{H\parallel y}$  at 0 T is smaller than  $R_{0T}^{H\parallel x}$ . Fig. 4(a) also demonstrates that such a field-driven switching process is repeatable. The signal difference  $\Delta R_{0T} (= R_{0T}^{H\parallel x} - R_{0T}^{H\parallel y})$  at zero field should be related to switching of the CoO AFM order, which is smaller than  $\Delta R_{9T} (= R_{9T}^{H\parallel x} - R_{9T}^{H\parallel y})$  measured at 9 T. Fig. 4(b) shows the measured MR ratios  $\Delta R_{0T}/R$  and  $\Delta R_{9T}/R$  as a function of temperature.  $\Delta R_{0T}/R$  represents the contribution due to the CoO AFM spin switching, and only exists between 150 K and 260 K with a maximum value of  $1.3 \times 10^{-4}$  at 190 K.  $\Delta R_{9T}/R$  is the SMR ratio measured at 9 T, which contains both effects of AFM spin switching and the applied field. The field effect on SMR can be quantified by subtracting  $\Delta R_{0T}/R$  from  $\Delta R_{9T}/R$ . The inset in Fig. 4(b) also shows the temperature-dependent  $\Delta R/R = (\Delta R_{9T} - \Delta R_{0T})/R$ , which can be fitted by an exponential decay function, so the field contribution on SMR is likely related to thermal excitation.

The field-driven switching of CoO AFM spins may depend on the film thickness, thus we prepared Pt/CoO/MgO(001) samples with the CoO layer growing into the step shape with different thicknesses, so all the samples with different CoO thicknesses were prepared under the same condition. Fig. 4(c) shows the measured temperature-dependent  $\Delta R_{0T}/R$  from three samples with  $d_{\text{CoO}}=2$  nm, 4 nm, and 8 nm.  $\Delta R_{0T}$  is quantified through the method described in Fig. 4(a), which shows the maximum peak at  $\sim 175$  K for the 8 nm CoO film. For thinner film, the SMR due to the AFM spin switching is observed in a narrower temperature range. As indicated in Fig. 3(c), the

---

decreasing of SMR switching signal at lower temperature can be attributed to the fact that the applied maximum field of 9 T is not strong enough to switch the CoO AFM spins. The switching field should be proportional to the magnetic anisotropy, which may decrease with the film thickness, thus the AFM spin switching can extend to lower temperatures for thicker CoO film. At higher temperature, the SMR switching signal decreases to zero at 220 K for the 2 nm CoO film, but extends to 260 K for the 4 nm and 8 nm CoO films. Moreover, the decreasing SMR signals for the 4 nm and 8 nm CoO films above 190 K are almost identical. We attribute the signal decrease above 190 K to the blocking temperature in the films, which has a certain relation with the Néel temperature  $T_N$  of the CoO film. In Ref. [44], the  $T_N$  of CoO film grown on MgO(001) increases with the film thickness, and the 2 nm CoO has the lower  $T_N$  of  $\sim 260$  K, but the  $T_N$  for the CoO film above 4 nm become almost saturated at  $\sim 300$  K. Thus, the SMR signal in Fig. 4(c) indicates that the blocking temperature is  $\sim 40$  K lower than  $T_N$ . Note that the applied current during MR measurements may slightly increase the sample temperature, but such current-induced temperature increase should be much less than 40 K.

#### D. Discussion on the origin of positive SMR

In general, the CoO film has the G-type AFM structure with the compensated spins in the CoO(001) plane, and due to the perpendicular coupling between the applied field and the AFM Néel order, the Pt/CoO layer is expected to generate a similar “negative” SMR with  $R_{\parallel} < R_{\perp}$  as that observed in the Pt/NiO bilayer [14-17,25]. Our experimental results show that the Pt/CoO bilayer only has the “positive” SMR with  $R_{\parallel} > R_{\perp}$ , indicating that the observed SMR is not directly related to the CoO AFM Néel order. The CoO film should contain many defects such as oxygen vacancy and surface roughness, so certain percentages of Co atoms at the Pt/CoO interface may have the valence state other than  $\text{Co}^{2+}$ , so it is possible that there are uncompensated spins at the Pt/CoO interface in addition to the CoO AFM spins with Néel order. According to the SMR theory for the HM/FMI system [2], those

---

interfacial uncompensated spins may induce the positive SMR.

In order to understand the temperature-dependent SMR signals at 9 T and 0 T in Fig. 4, we propose that the interfacial uncompensated CoO spins should be composed of two parts, as indicated in Fig. 5(a): one is the fixed spin strongly coupled with the AFM spins, and the other is the rotatable spin weakly coupled to the AFM spins. Those two types of spins may also associate with the reported fixed and rotatable CoO spins in the Fe/CoO bilayer as determined by XMLD [42]. Due to the spin-flop coupling, the fixed spins should be perpendicularly coupled to the CoO AFM spins, and can also be switched together with the CoO AFM spins induced by the applied field. No SMR contribution from the fixed spins can be observed at low temperature since the required switching field of the CoO AFM order is much larger than the applied field. Note that the fixed spins and the AFM spins with Néel order always rotate simultaneously. Our measurement can't separate the SMR contributions from the fixed spins and the AFM Néel order, but our results can suggest that the SMR signal induced by the fixed spins is much stronger than the possible “negative” SMR only due to the AFM Néel order.

The rotatable spins at the Pt/CoO interface may behave like the paramagnetic spins since they have weak crystalline anisotropy, thus the strong field can induce certain net spins, which are responsible for the observed strong SMR signal measured at 9 T shown in Figs. 3 and 4. Then, it is understandable that the related SMR signal in Fig. 4(b) has an exponential increase with decreasing temperature, since the Zeeman energy can better align the paramagnetic spins at lower temperature. The strong temperature-dependent positive SMR signal also indicates that the field-induced spins should not originate from the AFM spin structure. If the field-induced spins come from the CoO AFM spin structure, SMR signal should inversely depend on the magnetic anisotropy. Fig. 3(d) shows that the switching field increases with decreasing temperature, indicating that the CoO AFM spins have a stronger magnetic anisotropy energy at lower temperature, which can further reduce the field-induced spins. However, those effects are expected to suppress SMR signal at lower temperatures, and

---

cause a trend that is different from the inset in Fig. 4(b). On the other hand, if the field-induced SMR signal originates from the AFM spin structure, the ADMR signal should be quite different for the different spin orientations. Experimentally, we can align the AFM spins at 10 K either parallel or perpendicular to the current through the field cooling, and the measured SMR signals in these two cases have very little difference. So, the field-induced spin is related to the rotatable uncompensated spins instead of the AFM spin structure. **It is also worth to discuss the large SMR signal in Pt/CoO system, which is comparable to that in  $\text{Fe}_3\text{O}_2/\text{Pt}$  [45,46] and Rashba-Edelstein resistance in  $\alpha\text{-Fe}_3\text{O}_2/\text{TI}$ [47]. Previous study reported that spins in ultrathin NiFe films below the superparamagnetic limit has strong capabilities to absorb spins[48]. Therefore, it would be reasonable to expect that the paramagnetic-like rotatable spins also exhibit stronger spin-dependent absorption for the spins from Pt layer.**

The SMR signal due to the rotatable spins at the Pt/CoO interface can be observed even at a temperature above the  $T_N$  of CoO film [32]. Note that the SMR signal at 10 K in Fig. 4(b) is  $\sim 0.25\%$ , which is larger than that in Pt/YIG [1-4] and Pt/NiO systems [14,15] by one order of magnitude, and this SMR signal is even larger than the AMR in a 3 nm Co film grown on  $\text{Al}_2\text{O}_3(0001)$  [49]. Our SQUID measurement confirms that no FM moments can be observed in a 4 nm CoO film, consistent with the results in Ref. [19]. Such a large SMR signal at low temperature induced by the interfacial uncompensated spins can be confirmed experimentally. We prepared one sample of Pt/CoO bilayer with an interfacial CoO thickness of 0.02 nm ~~by with exposing~~, a very short time expose to the Co source. This amount of 0.02 nm CoO is only 10% coverage of one CoO monolayer, thus it is expected that only the CoO cluster with the uncompensated spins can form at the interface without any AFM order. Fig. 5(b) shows that such a small amount of CoO interface spins can induce the 0.24% MR, which is only slightly smaller than the value from the Pt/CoO(4 nm) bilayer prepared on the same MgO(001) substrate. Fig. 5(b) also shows the negligible ADMR signal from a Pt(3 nm)/MgO sample, which can exclude the possible contribution to the SMR signal in the Pt/CoO bilayer from the Hanle

---

magnetoresistance in the Pt layer [50].

#### IV. Summary

In summary, we systematically investigated the SMR effect in single crystalline Pt/CoO(001) bilayers. Utilizing the XMLD measurement, we demonstrated that the field cooling can align the CoO AFM Néel order perpendicular to the field for the cooling field along CoO<110> directions, and the CoO AFM spins can be orthogonally switched while applying the strong field parallel to the CoO AFM spins at proper temperatures. The ADMRs in Pt/CoO bilayers show a positive angular dependence with  $R_{\parallel} > R_{\perp}$ , opposite to the SMR in Pt/NiO systems. Our measurements separated the SMR contributions related to the switching of the CoO Néel order and the field induced spins, and both contributions contain a positive SMR. The SMR contribution related to switching of the CoO Néel order only exist in a narrow temperature range below  $T_N$ , but the field-induced SMR signal strongly increases with decreasing temperature. The observed positive SMRs can be interpreted by two types of uncompensated spins at the Pt/CoO interface, which are either strongly or weakly coupled with the CoO AFM spins. Our results should attract great interest for understanding the complicated spin-dependent transport properties related to AFM materials.

#### Acknowledgements:

The work was supported by the National Natural Science Foundation of China (Grant No. [11974079](#)~~11734006~~, ~~and~~ No. [11734006](#), No. [12274083](#) and No. [12221004](#)~~11974079~~) and the Shanghai Municipal Science and Technology Major Project (Grant No. 2019SHZDZX01). This research also used the resources of Advanced Light Source, which is a DOE Office of Science User Facility. Jia Xu and Chao Zhou acknowledge support by Natural Science Basic Research Program of Shaanxi (Grant No. 2022JQ-017), Natural Science Foundation of Shaanxi Provincial Department of Education (Grant No. 22JK0310 and No. 22JK0321) and Shaanxi University of Technology (SLGRCQD2125). Qian Li and Mengmeng Yang also acknowledge

---

support by excellence program of Hefei Science Center CAS (No. 2021HSC-UE003), National Natural Science Foundation of China (Grant No. 12174364 and No. 12104003), Natural Science Foundation of Anhui Province (Grant No. 2108085QA20), the Fundamental Research Funds for the Central Universities (No. wk2310000104). Gong Chen acknowledges support by the US NSF (DMR-2005108). Ziqiang Qiu acknowledges support by US Department of Energy, Office of Science, Office of Basic Energy Sciences, Materials Sciences and Engineering Division under Contract No. DE-AC02-05CH11231 (van der Waals heterostructures program, KCWF16).

### Reference :

- [1] H. Nakayama, M. Althammer, Y. T. Chen, K. Uchida, Y. Kajiwara, D. Kikuchi, T. Ohtani, S. Geprags, M. Opel, S. Takahashi, R. Gross, G. E. Bauer, S. T. Goennenwein, and E. Saitoh, Spin Hall magnetoresistance induced by a nonequilibrium proximity effect, *Phys. Rev. Lett.* **110**, 206601 (2013).
- [2] Y.-T. Chen, S. Takahashi, H. Nakayama, M. Althammer, S. T. B. Goennenwein, E. Saitoh, and G. E. W. Bauer, Theory of spin Hall magnetoresistance, *Phys. Rev. B* **87**, 144411 (2013).
- [3] M. Althammer, S. Meyer, H. Nakayama, M. Schreier, S. Altmannshofer, M. Weiler, H. Huebl, S. Geprags, M. Opel, R. Gross, D. Meier, C. Klewe, T. Kuschel, J.-M. Schmalhorst, G. Reiss, L. Shen, A. Gupta, Y.-T. Chen, G. E. W. Bauer, E. Saitoh, and S. T. B. Goennenwein, Quantitative study of the spin Hall magnetoresistance in ferromagnetic insulator/normal metal hybrids, *Phys. Rev. B* **87**, 224401 (2013).
- [4] N. Vlietstra, J. Shan, V. Castel, B. J. van Wees, and J. Ben Youssef, Spin-Hall magnetoresistance in platinum on yttrium iron garnet: dependence on platinum thickness and in-plane/out-of-plane magnetization, *Phys. Rev. B* **87**, 184421 (2013).
- [5] Z. Ding, B. L. Chen, J. H. Liang, J. Zhu, J. X. Li, and Y. Z. Wu, Spin Hall magnetoresistance in Pt/Fe<sub>3</sub>O<sub>4</sub> thin films at room temperature, *Phys. Rev. B* **90**, 134424 (2014).
- [6] J. M. Gomez-Perez, X. P. Zhang, F. Calavalle, M. Ilyn, C. Gonzalez-Orellana, M. Gobbi, C. Rogero, A. Chuvilin, V. N. Golovach, L. E. Hueso, F. S. Bergeret, and F. Casanova, Strong interfacial exchange field in a heavy metal/ferromagnetic insulator system determined by spin Hall magnetoresistance, *Nano Lett.* **20**, 6815 (2020).
- [7] J. Kim, P. Sheng, S. Takahashi, S. Mitani, and M. Hayashi, Spin Hall magnetoresistance in metallic bilayers, *Phys. Rev. Lett.* **116**, 097201 (2016).
- [8] X. Xiao, J. X. Li, Z. Ding, J. H. Liang, L. Sun, and Y. Z. Wu, Unusual angular dependent magnetoresistance in single-crystalline Co/Pt bilayers, *Appl. Phys. Lett.* **108**, 222402 (2016).
- [9] M. Kawaguchi, D. Towa, Y.-C. Lau, S. Takahashi, and M. Hayashi, Anomalous spin Hall magnetoresistance in Pt/Co bilayers, *Appl. Phys. Lett.* **112**, 202405 (2018).
- [10] M. Isasa, A. Bedoya-Pinto, S. Vélez, F. Golmar, F. Sánchez, L. E. Hueso, J. Fontcuberta, and



---

F. Casanova, Spin Hall magnetoresistance at Pt/CoFe<sub>2</sub>O<sub>4</sub> interfaces and texture effects, *Appl. Phys. Lett.* **105**, 142402 (2014).

[11] K. Ganzhorn, J. Barker, R. Schlitz, B. A. Piot, K. Ollefs, F. Guillou, F. Wilhelm, A. Rogalev, M. Opel, M. Althammer, S. Geprägs, H. Huebl, R. Gross, G. E. W. Bauer, and S. T. B. Goennenwein, Spin Hall magnetoresistance in a canted ferrimagnet, *Phys. Rev. B* **94**, 094401 (2016).

[12] A. Aqeel, N. Vlietstra, A. Roy, M. Mostovoy, B. J. van Wees, and T. T. M. Palstra, Electrical detection of spiral spin structures in Pt|Cu<sub>2</sub>OSeO<sub>3</sub> heterostructures, *Phys. Rev. B* **94**, 134418 (2016).

[13] W. Zhang, M. B. Jungfleisch, W. Jiang, J. E. Pearson, A. Hoffmann, F. Freimuth, and Y. Mokrousov, Spin Hall effects in metallic antiferromagnets, *Phys. Rev. Lett.* **113**, 196602 (2014).

[14] L. Baldrati, A. Ross, T. Niizeki, C. Schneider, R. Ramos, J. Cramer, O. Gomonay, M. Filianina, T. Savchenko, D. Heinze, A. Kleibert, E. Saitoh, J. Sinova, and M. Kläui, Full angular dependence of the spin Hall and ordinary magnetoresistance in epitaxial antiferromagnetic NiO(001)/Pt thin films, *Phys. Rev. B* **98**, 024422 (2018).

[15] J. Fischer, O. Gomonay, R. Schlitz, K. Ganzhorn, N. Vlietstra, M. Althammer, H. Huebl, M. Opel, R. Gross, S. T. B. Goennenwein, and S. Geprags, Spin Hall magnetoresistance in antiferromagnet/heavy-metal heterostructures, *Phys. Rev. B* **97**, 014417 (2018).

[16] X. Z. Chen, R. Zarzuela, J. Zhang, C. Song, X. F. Zhou, G. Y. Shi, F. Li, H. A. Zhou, W. J. Jiang, F. Pan, and Y. Tserkovnyak, Antidamping-torque-induced switching in biaxial antiferromagnetic insulators, *Phys. Rev. Lett.* **120**, 207204 (2018).

[17] T. Moriyama, K. Oda, T. Ohkochi, M. Kimata, and T. Ono, Spin torque control of antiferromagnetic moments in NiO, *Sci. Rep.* **8**, 14167 (2018).

[18] Y. Cheng, S. Yu, M. Zhu, J. Hwang, and F. Yang, Electrical switching of tristate antiferromagnetic Néel order in  $\alpha$ -Fe<sub>2</sub>O<sub>3</sub> epitaxial films, *Phys. Rev. Lett.* **124**, 027202 (2020).

[19] L. Baldrati, C. Schmitt, O. Gomonay, R. Lebrun, R. Ramos, E. Saitoh, J. Sinova, and M. Klau, Efficient spin torques in antiferromagnetic CoO/Pt quantified by comparing field- and current-induced switching, *Phys. Rev. Lett.* **125**, 077201 (2020).

[20] J. E. Hirsch, Spin Hall Effect, *Phys. Rev. Lett.* **83**, 1834 (1999).

[21] S. Zhang, Spin hall effect in the presence of spin diffusion, *Phys. Rev. Lett.* **85**, 393 (2000).

[22] T. Shang, Q. F. Zhan, H. L. Yang, Z. H. Zuo, Y. L. Xie, L. P. Liu, S. L. Zhang, Y. Zhang, H. H. Li, B. M. Wang, Y. H. Wu, S. Zhang, and R.-W. Li, Effect of NiO inserted layer on spin-Hall magnetoresistance in Pt/NiO/YIG heterostructures, *Appl. Phys. Lett.* **109**, 032410 (2016).

[23] D. Hou, Z. Qiu, J. Barker, K. Sato, K. Yamamoto, S. Velez, J. M. Gomez-Perez, L. E. Hueso, F. Casanova, and E. Saitoh, Tunable sign change of spin Hall magnetoresistance in Pt/NiO/YIG structures, *Phys. Rev. Lett.* **118**, 147202 (2017).

[24] W. Lin and C. L. Chien, Electrical detection of spin backflow from an antiferromagnetic insulator/Y<sub>3</sub>Fe<sub>5</sub>O<sub>12</sub> interface, *Phys. Rev. Lett.* **118**, 067202 (2017).

[25] G. R. Hoozeboom, A. Aqeel, T. Kuschel, T. T. M. Palstra, and B. J. van Wees, Negative spin Hall magnetoresistance of Pt on the bulk easy-plane antiferromagnet NiO, *Appl. Phys. Lett.* **111**, 052409 (2017).

[26] R. Lebrun, A. Ross, O. Gomonay, S. A. Bender, L. Baldrati, F. Kronast, A. Qaiumzadeh, J. Sinova, A. Brataas, R. A. Duine, and M. Kläui, Anisotropies and magnetic phase transitions in insulating antiferromagnets determined by a Spin-Hall magnetoresistance probe, *Communications Physics* **2**, 50 (2019).

[27] Y. Ji, J. Miao, K. K. Meng, Z. Y. Ren, B. W. Dong, X. G. Xu, Y. Wu, and Y. Jiang, Spin Hall

---

magnetoresistance in an antiferromagnetic magnetoelectric Cr<sub>2</sub>O<sub>3</sub>/heavy-metal W heterostructure, *Appl. Phys. Lett.* **110**, 262401 (2017).

[28] R. Schlitz, T. Kosub, A. Thomas, S. Fabretti, K. Nielsch, D. Makarov, and S. T. B. Goennenwein, Evolution of the spin hall magnetoresistance in Cr<sub>2</sub>O<sub>3</sub>/Pt bilayers close to the Néel temperature, *Appl. Phys. Lett.* **112**, 132401 (2018).

[29] J. Qin, D. Hou, Y. Chen, E. Saitoh, and X. Jin, Spin Hall magnetoresistance in Pt/Cr<sub>2</sub>O<sub>3</sub>/YIG structure, *J. Magn. Magn. Mater.* **534**, 167980 (2021).

[30] L. Huang, Y. Zhou, T. Guo, F. Pan, and C. Song, Tunable spin Hall magnetoresistance in all-antiferromagnetic heterostructures, *Chinese Physics Letters* **39**, 047502 (2022).

[31] Y. Ji, J. Miao, Y. M. Zhu, K. K. Meng, X. G. Xu, J. K. Chen, Y. Wu, and Y. Jiang, Negative spin Hall magnetoresistance in antiferromagnetic Cr<sub>2</sub>O<sub>3</sub>/Ta bilayer at low temperature region, *Appl. Phys. Lett.* **112**, 232404 (2018).

[32] K. Oda, T. Moriyama, M. Kimata, S. Kasukawa, and T. Ono, Temperature dependence of spin Hall magnetoresistance across the Néel temperature of CoO, *Jpn. J. Appl. Phys.* **59**, 010908 (2020).

[33] S. Y. Bodnar, Y. Skourski, O. Gomonay, J. Sinova, M. Kläui, and M. Jourdan, Magnetoresistance effects in the metallic antiferromagnet Mn<sub>2</sub>Au, *Phys. Rev. Appl.* **14**, 014004 (2020).

[34] R. Abrudan, J. Miguel, M. Bernien, C. Tieg, M. Piantek, J. Kirschner, and W. Kuch, Structural and magnetic properties of epitaxial Fe/CoO bilayers on Ag(001), *Phys. Rev. B* **77**, 014411 (2008).

[35] J. Wu, D. Carlton, J. S. Park, Y. Meng, E. Arenholz, A. Doran, A. T. Young, A. Scholl, C. Hwang, H. W. Zhao, J. Bokor, and Z. Q. Qiu, Direct observation of imprinted antiferromagnetic vortex states in CoO/Fe/Ag(001) discs, *Nat. Phys.* **7**, 303 (2011).

[36] J. Xu, H. Chen, C. Zhou, D. Shi, G. Chen, and Y. Wu, Optical imaging of antiferromagnetic domains in ultrathin CoO(001) films, *New J. Phys.* **22**, 083033 (2020).

[37] J. Miguel, R. Abrudan, M. Bernien, M. Piantek, C. Tieg, J. Kirschner, and W. Kuch, Magnetic domain coupling study in single-crystalline Fe/CoO bilayers, *J. Phys. Condens. Matter* **21**, 185004 (2009).

[38] Q. Li, G. Chen, T. P. Ma, J. Zhu, A. T. N'Diaye, L. Sun, T. Gu, Y. Huo, J. H. Liang, R. W. Li, C. Won, H. F. Ding, Z. Q. Qiu, and Y. Z. Wu, Activation of antiferromagnetic domain switching in exchange-coupled Fe/CoO/MgO(001) systems, *Phys. Rev. B* **91**, 134428 (2015).

[39] J. Xu, J. Xia, X. Zhang, C. Zhou, D. Shi, H. Chen, T. Wu, Q. Li, H. Ding, Y. Zhou, and Y. Wu, Exchange-torque-triggered fast switching of antiferromagnetic domains, *Phys. Rev. Lett.* **128**, 137201 (2022).

[40] M. J. Grzybowski, C. F. Schippers, M. E. Bal, K. Rubi, U. Zeitler, M. Foltyn, B. Koopmans, and H. J. M. Swagten, Electrical switching of antiferromagnetic CoO|Pt across the Néel temperature, *Appl. Phys. Lett.* **120**, 122405 (2022).

[41] Q. Li, T. Gu, J. Zhu, Z. Ding, J. X. Li, J. H. Liang, Y. M. Luo, Z. Hu, C. Y. Hua, H. J. Lin, T. W. Pi, C. Won, and Y. Z. Wu, Multiple in-plane spin reorientation transitions in Fe/CoO bilayers grown on vicinal MgO(001), *Phys. Rev. B* **91**, 104424 (2015).

[42] J. Wu, J. S. Park, W. Kim, E. Arenholz, M. Liberati, A. Scholl, Y. Z. Wu, C. Hwang, and Z. Q. Qiu, Direct measurement of rotatable and frozen CoO spins in exchange bias system of CoO/Fe/Ag(001), *Phys. Rev. Lett.* **104**, 217204 (2010).

[43] Q. Li, T. P. Ma, M. Yang, L. Sun, S. Y. Huang, R. W. Li, C. Won, Z. Q. Qiu, and Y. Z. Wu, Field dependence of antiferromagnetic domain switching in epitaxial Fe/CoO/MgO(001) systems, *Phys.*

---

Rev. B **96**, 024420 (2017).

[44] E. N. Abarra, K. Takano, F. Hellman, and A. E. Berkowitz, Thermodynamic measurements of magnetic ordering in antiferromagnetic superlattices, *Phys. Rev. Lett.* **77**, 3451 (1996).

[45] Y. J. Zhou, X. Z. Chen, X. F. Zhou, H. Bai, R. Y. Chen, F. Pan, and C. Song, A comparative study of spin Hall magnetoresistance in Fe<sub>2</sub>O<sub>3</sub>-based systems, *J. Appl. Phys.* **127**, 163904 (2020).

[46] J. Fischer, M. Althammer, N. Vlietstra, H. Huebl, S. T. B. Goennenwein, R. Gross, S. Geprägs, and M. Opel, Large Spin Hall Magnetoresistance in Antiferromagnetic  $\alpha$ -Fe<sub>2</sub>O<sub>3</sub>/Pt Heterostructures, *Physical Review Applied* **13** (2020).

[47] Y. Lv, J. Kally, T. Liu, P. Quarterman, T. Pillsbury, B. J. Kirby, A. J. Grutter, P. Sahu, J. A. Borchers, M. Wu, N. Samarth, and J.-P. Wang, Large unidirectional spin Hall and Rashba–Edelstein magnetoresistance in topological insulator/magnetic insulator heterostructures, *Applied Physics Reviews* **9**, 011406 (2022).

[48] C. J. Durrant, L. R. Shelford, R. A. J. Valkass, R. J. Hicken, A. I. Figueroa, A. A. Baker, G. van der Laan, L. B. Duffy, P. Shafer, C. Klewe, E. Arenholz, S. A. Cavill, J. R. Childress, and J. A. Katine, Dependence of spin pumping and spin transfer torque upon Ni<sub>81</sub>Fe<sub>19</sub> thickness in Ta/Ag/Ni<sub>81</sub>Fe<sub>19</sub>/Ag/Co<sub>2</sub>MnGe/Ag/Ta spin-valve structures, *Phys. Rev. B* **96**, 144421 (2017).

[49] M. Jia, F. Zeng, X. Xiao, C. Zhou, X. Hu, and Y. Wu, Thickness-dependent angular dependent magnetoresistance in single-crystalline Co film and Co/Pt heterostructures, *J. Magn. Magn. Mater.* **508**, 166863 (2020).

[50] S. Velez, V. N. Golovach, A. Bedoya-Pinto, M. Isasa, E. Sagasta, M. Abadia, C. Rogero, L. E. Hueso, F. S. Bergeret, and F. Casanova, Hanle magnetoresistance in thin metal films with strong spin-orbit coupling, *Phys. Rev. Lett.* **116**, 016603 (2016).

Figures:

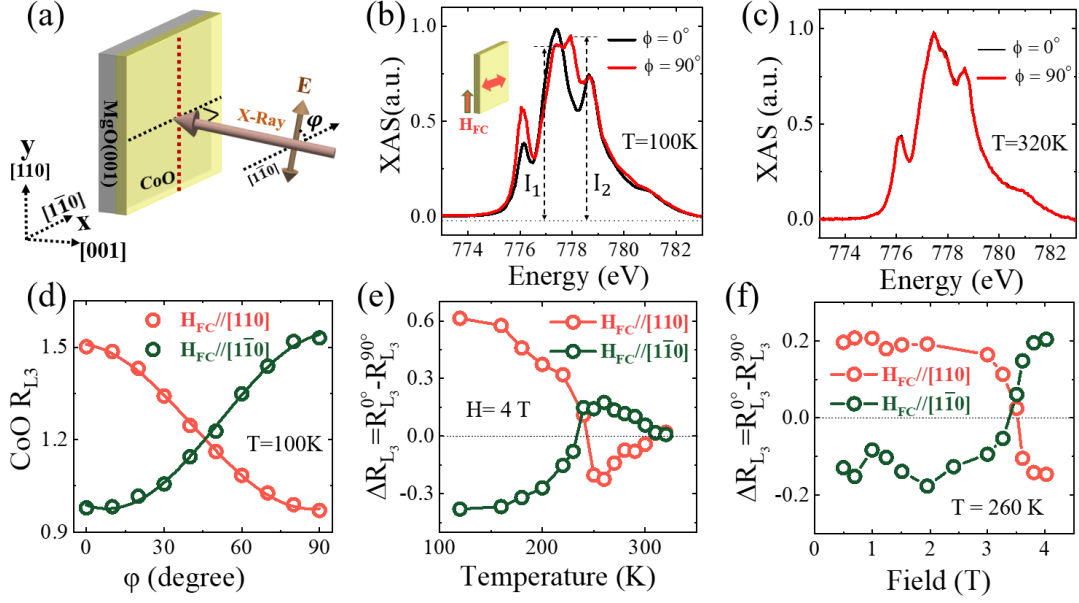


**Fig. 1.** (a) Schematic drawings of the XMLD measurement geometry. (b) Representative XAS spectra of the  $\text{Co}^{2+} L_3$  edge at  $T=100$  K after field cooling with  $H_{FC} \parallel \text{CoO}[110]$  from a Pt (1.2nm)/CoO (4nm)/MgO(001) sample. (c) XAS spectra of the  $\text{Co}^{2+} L_3$  edge at  $T=320$  K above the CoO Néel temperature. (d) The  $\varphi$ -dependent  $\text{CoO } R_{L_3}$  at  $T=100$  K after field cooling with  $H_{FC} \parallel [110]$  and  $H_{FC} \parallel [1\bar{1}0]$ . The solid lines represent the fitting by the  $\cos(2\varphi)$  function. (e) The  $L_3$  ratio difference  $\Delta R_{L_3}$  as a function of temperature under a field of 4 T. (f) The field-dependent  $\Delta R_{L_3}$  evolution at  $T=260$  K for  $H \perp H_{FC}$ .



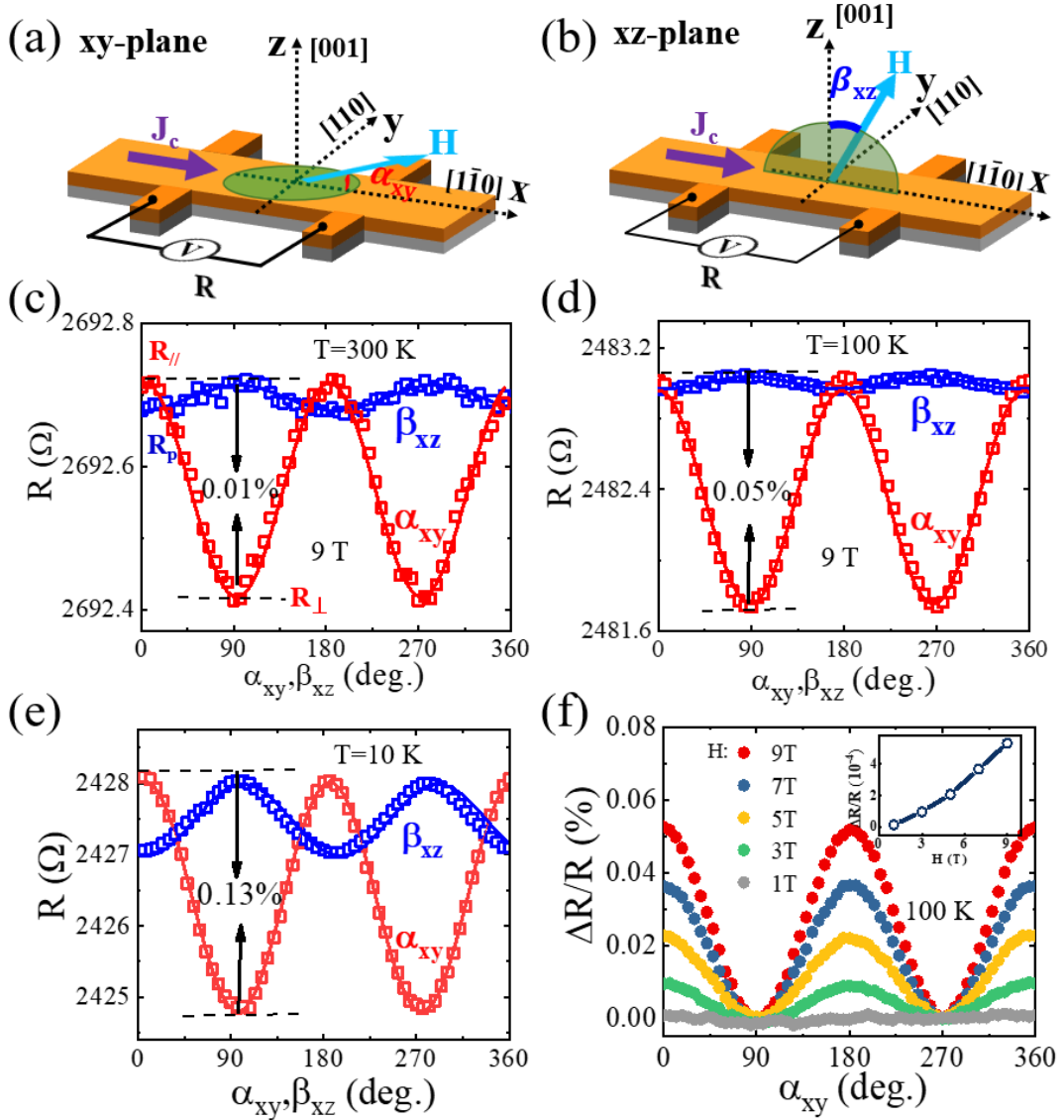


**Fig. 2.** (a)-(b) Geometries of angular-dependent MR measurements with field rotating in (a) the xy-plane and (b) the xz-plane. (c)-(e) Angular-dependent MR in the Pt (3 nm)/CoO(4 nm) film within a rotating field of 9 T at (c) 300 K, (d) 100 K and (e) 10 K. (f) ADMR curves in  $\alpha_{xy}$  scan with different field strengths at 100 K. The inset shows the measured ADMR ratio as a function of field strength.

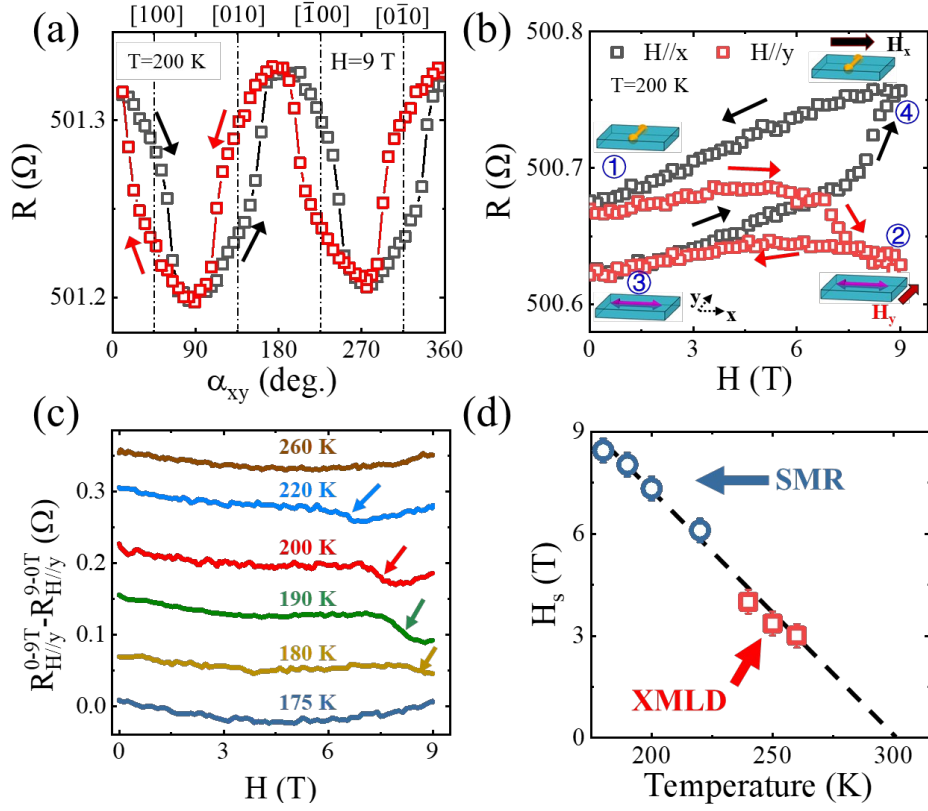


**Fig. 3.** (a) ADMR curves of a Pt (3 nm)/CoO(4 nm) film measured at 200 K in  $\alpha_{xy}$ -scan with a 9 T field rotating clockwise and anticlockwise. (b) Field-dependent MR signal at 200 K after field cooling with  $H_{FC} // x$ . (c) The MR difference at different temperatures between the loops with the field  $H_y$  increasing or decreasing shown in (b). (d) Temperature-dependent switching field  $H_s$  of CoO AFM spins for the 4 nm CoO(001) film. The blue dots are derived from the MR measurement in (c), and red squares are obtained from the XMLD results in Fig. 1. The black line is a visual guide.

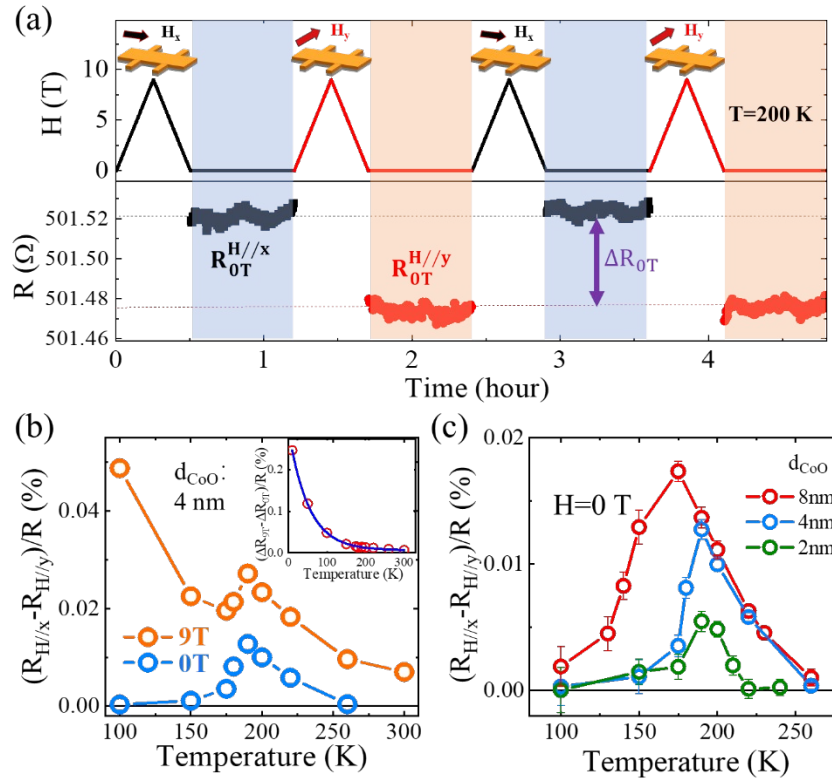


**Fig. 4.** (a) Time-dependent MR under an alternating field sequence at 200 K measured from a Pt(3 nm)/CoO(4 nm) film. The magnetic field directions are shown as arrows, and the MR is measured at zero field. (b) Temperature-dependent MR ratios measured with fields of 0 T and 9 T, respectively. The insert shows the temperature-dependent difference between the MR ratios measured at 0 T and 9 T, and the solid line is the fitting with an exponential decay function. (c) Temperature-dependent ratios measured at zero field from the Pt(3 nm)/CoO samples with different CoO thicknesses.



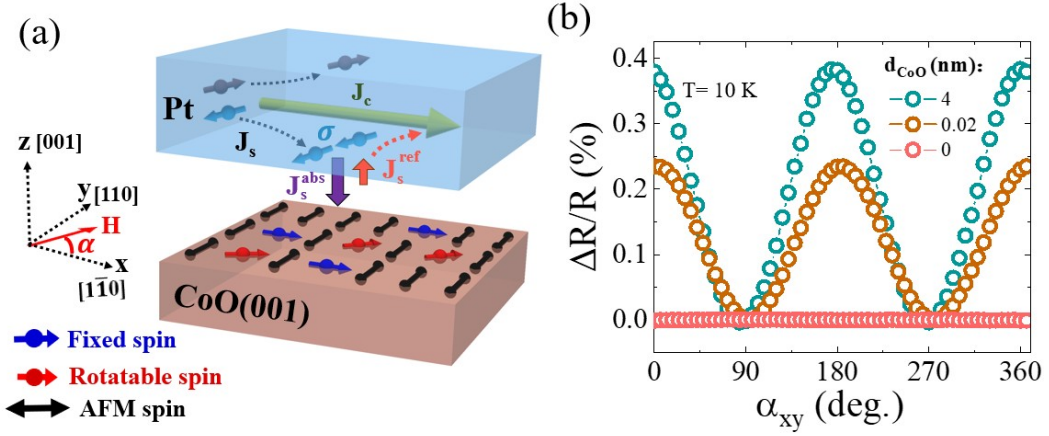


**Fig. 5.** (a) Schematic drawing of the compensated AFM spins, fixed and rotatable uncompensated spins at the CoO/Pt interface. The spin current in the Pt layer generated by the SHE effect is reflected at the interface and generates the SMR effect. (b) ADMR curves in the Pt(3 nm)/CoO bilayers with different CoO thicknesses measured at 10 K with a 9 T rotating field in  $\alpha_{xy}$  scan.